DTU Library

High coincidence-to-accidental ratio continuous-wave photon-pair generation in a grating-coupled silicon strip waveguide

Letters

Guo, Kai; Christensen, Erik Nicolai; Christensen, Jesper Bjerge; Koefoed, Jacob Gade; Bacco, Davide; Ding, Yunhong; Ou, Haiyan; Rottwitt, Karsten

Published in:
Applied Physics Express

Link to article, DOI:
10.7567/APEX.10.062801

Publication date:
2017

Document Version
Peer reviewed version

High coincidence-to-accidental ratio continuous-wave photon-pair generation in a grating-coupled silicon strip waveguide

Kai Guo [1,2] *, Erik N. Christensen [2], Jesper B. Christensen[2], Jacob G. Koefoed[2], Davide Bacco [2], Yunhong Ding [2], Haiyan Ou [2] and Karsten Rottwitt[2]

[1] *College of Opto-Electronics Science and Engineering, National University of Defense Technology, Deya Road 109, Changsha, Hunan, China*

Department of Photonics Engineering, Technical University of Denmark, Ørsteds Plads 343, Kgs. Lyngby, Denmark

We demonstrate a very high coincidence-to-accidental ratio of 673 by using continuous-wave photon-pair generation in a silicon strip waveguide through spontaneous four-wave mixing. This is achieved by employing on-chip photonic crystal based grating couplers for both low-loss fiber-to-chip coupling and on-chip generated noise spontaneous Raman scattering suppression. We measure a minimum heralded second-order correlation of $g_{\mathrm{H}}^{(2)}(0) = 0.12$, demonstrating that our source operates in the single-photon regime with low noise.

Quantum correlated photon pairs is a key resource in quantum optics research and applications e.g. quantum computing and quantum communication [1, 2]. Sources capable of producing such pairs are commonly realized by nonlinear optical phenomena such as spontaneous parametric down-conversion in second-order nonlinear media [3, 4], or spontaneous four-wave mixing (SpFWM) in third-order nonlinear media [5, 6, 7, 8, 9, 10, 11, 12, 13, 14, 15]. While the majority of initial experiments were carried out using optical crystals [3], quasi-phase matched waveguides [4], or various optical fiber designs [5, 6], the last decade has seen a transition towards using miniaturized waveguide platforms. As a result, correlated photon-pair sources have been demonstrated in integrated platforms of crystalline silicon [7, 8, 9], amorphous silicon [10], silica[11], silicon-nitride [12], chalcogenide [13], and AlGaAs [14].

The silicon-on-insulator (SOI) waveguide platform is of particular interest due to its compatibility with complementary metal-oxide semiconductor (CMOS) technology and the mature fabrication methods allowing for reliable and reproducible results. The CMOS-compatibility is an especially appealing feature of SOI photonics as it enables advanced on-chip integration of various electrically or optically controlled components [16]. Furthermore,

*E-mail: guokai07203@hotmail.com

the capability of dispersion engineering through careful geometrical design, with a small footprint due to application of a high refractive index contrast material, makes SOI waveguides a natural platform for nonlinear optics [17]. The nonlinear response of silicon, however, also includes effects such as Raman scattering. Whereas spontaneous Raman scattering (SpRS) presents a serious noise source in amorphous silica, i.e. optical fibers, the main part of the silicon Raman response is a narrow-band peak located at a frequency shift of 15.6 THz, allowing easy filtering [18].

The arguably most mature technology in quantum information science is quantum key distribution (QKD) [19, 20, 21]. Many schemes for enabling this technology require sources that emit single photons with low noise contamination, preferably at telecom wavelengths for low-loss propagation in optical fiber networks. Moreover, for QKD, it often suffices that the single photons are emitted in a probabilistic manner, as long as a trigger signal is provided. This can be achieved simply by using a signal-idler photon-pair source, and letting the detection of the idler photon herald the presence of the signal photon, or vice versa. Such a heralded single-photon source can be constructed by using a continuous-wave (CW) pump laser to drive the photon-pair generation [22, 23]. CW lasers are cheaper, more compact, and more easily integrated on chip, than the pulsed laser alternative [22]. On the other hand, the narrow spectral linewidth of CW lasers lead to strong spectral anti-correlation in the signal-idler photon pair, which upon heralding projects the remaining single-photon into a spectral classical mixture [24, 25]. While such spectral anti-correlation may sometimes be desired, as it enables time-energy entanglement [26, 27, 21, 28, 29, 30], it can easily be avoided by spectral filtering, or it can be used to construct multiple wavelength channels of correlated signal-idler photon pairs [31]. Furthermore, a CW-pumped photon-pair source can be used not only for QKD purposes, but also for other quantum protocols, like covert quantum communications and quantum secure direct communications, where the uncertainty of the photon-pair arrival time is used as a degree of freedom[32, 33].

In this work, we demonstrate a CW pumped source of correlated photon pairs based on SpFWM in a silicon strip waveguide. The source utilizes a pair of photonic crystal based grating couplers (PCGCs) to effectively couple light in and out of the chip [34]. The PCGCs have a 3 dB transmission spectrum ranging from 1538 nm to 1567 nm, and the silicon Raman line is filtered by a minimum of 11 dB in the out-coupling grating. To characterize the source, the coincidence-to-accidental ratio (CAR) and the heralded second-order correlation $g^{(2)}_{\mathrm{H}}$ is measured, and the pair brightness is calculated. By utilizing PCGCs and thorough filtering it has been possible for us to achieve a record high CAR of 673.

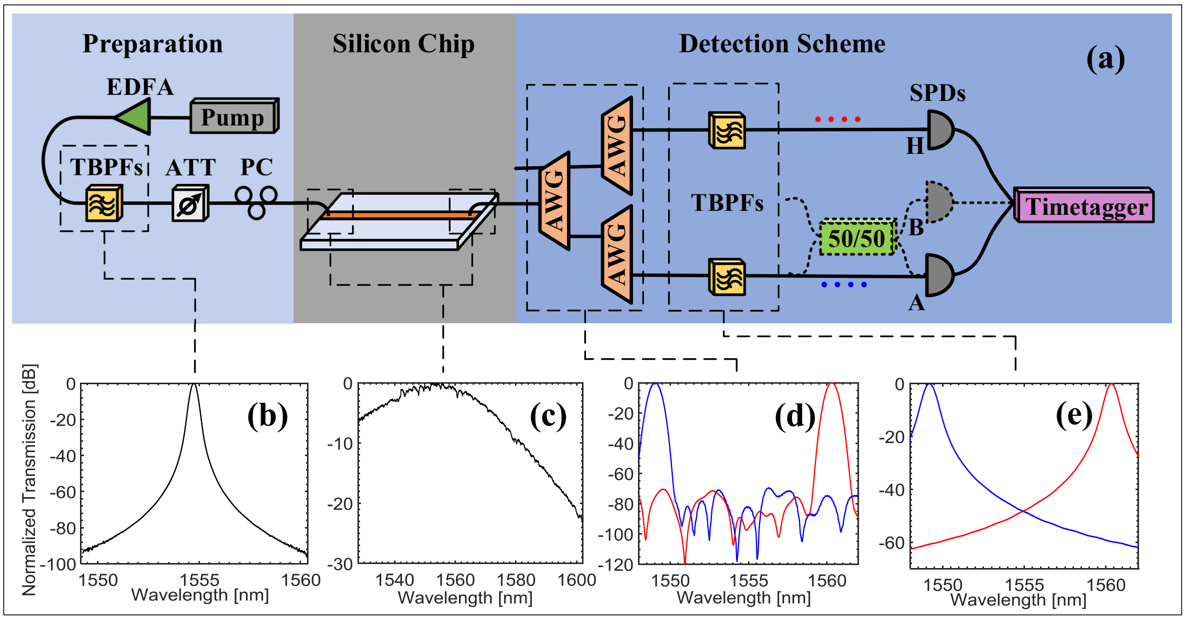

Fig. 1. (a) Schematic of the experimental setup comprised of pump preparation, silicon waveguide, and detection scheme. The detection scheme can be configured for a coincidence measurement between detectors A and H (solid lines) or a second-order correlation measurement, which in addition requires a 50/50 coupler and an extra detector B (dashed lines). Measured normalized transmission spectra are shown for (b) two cascaded tunable band-pass filters for pump preparation, (c) the combined in-out photonic crystal based grating couplers, (d) the arrayed waveguide gratings, and (e) tunable band-pass filters for pump suppression. EDFA: Erbium-doped fiber amplifier, TBPF: Tunable band-pass filter, ATT: Tunable attenuator, PC: Polarization controller, AWG: Arrayed waveguide grating, SPD: Single-photon detector.

A schematic of the experimental set up is shown in Fig. 1. A narrow-bandwidth CW laser, with a central wavelength of 1554.75 nm, is amplified to 25 dBm by an erbium-doped fiber amplifier (EDFA) and used to pump the SpFWM process. Two cascaded tunable band-pass filters (TBPFs) are employed to suppress the pump side-band noise resulting in an extinction ratio of 90 dB at a detuning of ±5 nm from the pump wavelength, see Fig. 1(b). A tunable attenuator is applied to adjust the pump power, ensuring that the pump signal to noise ratio (SNR) is constant, and a polarization controller (PC) is used to align the polarization angle to maximize coupling of the pump into the waveguide. The in-out coupling single-mode fibers are held by 75° vertical holders and are aligned with the PCGCs. The dimension of the silicon waveguide is $H \times W \times L = 250$ nm $\times$ 450 nm $\times$ 1 cm, covered by silica with a thickness around 1 μm. Using a finite-difference mode solver, the group-velocity dispersion parameter β_2 and the nonlinear coefficient γ are estimated to be -1.4 ps^2 m^{-1} and 300 (W m)$^{-1}$, respectively[35, 36]. Using a cut-back method, the waveguide was measured to have a coupling loss of 9 dB with a linear loss of 2 dB/cm for all wavelengths of interest. After the waveguide, arrayed waveguide gratings (AWGs) are used to filter out the pump field and separate the signal and idler into two arms, see Fig. 1(d), in which additional TBPFs are used to remove any remaining pump leakage, see Fig. 1(e). The central wavelengths of the signal and idler are 1560.4 nm and 1549.2 nm, respectively, both with a spectral full-width half-maximum (FWHM) width of 0.4 nm. Note that the signal and the idler wavelengths originate from a FWM spectrum with a 3 dB width of 36 nm. The photons are detected by two free-running single-photon detectors (SPD, ID230) with dark count rates of 50 Hz, collection efficiencies of 20 %, and dead times of 10 µs. Finally, the coincidental-temporal histogram is calculated through a time-tagging unit (ID801).

The noise in the system is comprised of SpRS, pump-amplified spontaneous emission (ASE) side-band noise, pump leakage, and dark counts from the detectors. To achieve a high CAR, the background noise should be extinguished to a level of −140 dBm. This corresponds to a photon rate, which is close to the noise floor of 50 Hz in the detectors. The SpRS from the silicon waveguide is filtered by the out-coupling PCGC with a minimum insertion loss of 11 dB, which is verified by measuring the broadband spectrum, see Fig. 1(c). This on-chip filtering of SpRS is not achieved in more broadband PCGCs or when using butt-coupling with lensed fiber. The pump SNR is approximately 150 dB, which is achieved by launching a strong seed to the EDFA, and using TBPFs to quench the side-band noise. Pump photons are removed by a cascade of AWGs and TBPFs, where the signal and idler are also separated. After propagation through the system, the side-band noise and pump leakage are at −140 dBm.

To quantify the photon-pair SNR, the CAR is calculated as

$$\mathrm{CAR} = \frac{N_{\mathrm{cc}} - N_{\mathrm{acc}}}{N_{\mathrm{acc}}}, \tag{1}$$

where N_{cc} is the raw coincidence counts between detector H and A, see Fig. 1, while N_{acc} is the accidental coincidence counts. They are obtained through the coincidental-temporal histogram as seen in the inset in Fig. 2, where the coincidence counts is the peak, and the accidental counts is the averaged background. The width of the peak is determined by the detector timing jitter of 300 ps, and thus in the CW regime the obtainable CAR is directly limited by the detector jitter. This is in contrast to a pulsed pump configuration, where the CAR in most cases is limited by the pump pulse duration [6].

In Fig. 2 the CAR is shown as a function of pump power. The peak CAR is 673 at a nonlinear phase shift of $\Phi_{\mathrm{NL}} = \gamma P_{\mathrm{p}} L_{\mathrm{eff}} \approx 4 \times 10^{-4}$, where $L_{\mathrm{eff}} = (1 - \mathrm{e}^{-\alpha L})/\alpha$ is the effective waveguide length and α is the linear propagation loss. Usually the maximum CAR is obtained

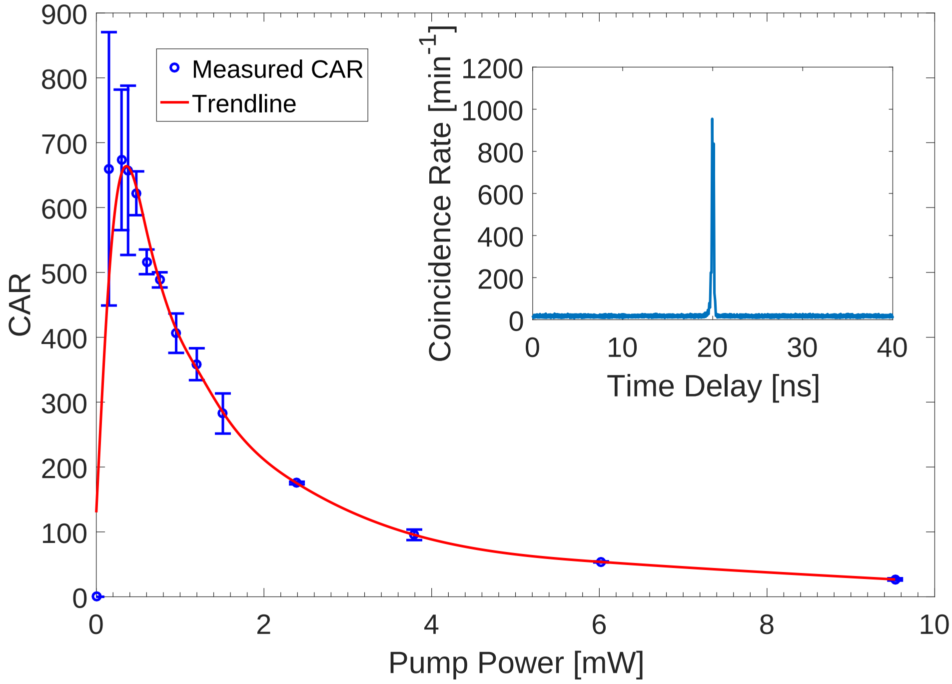

Fig. 2. CAR measurement at a range of pump powers. Inset shows coincidence histogram between detectors H and A at 9.5 mW pump power.

at a larger value of Φ_{NL} [37, 15], and this therefore directly illustrates the effective noise suppression in our experiment. The CAR is reduced to 26 at P_{p} = 9.5 mW, which is still an acceptable noise figure for e.g. QKD [21, 19, 20].

The coincidence and accidental coincidence counts are shown in Fig. 3. The coincidence counts has a fitted slope of 1.81, which is consistent with the pair rate being proportional to Φ_{NL}^2 [38]. The point corresponding to the highest pump power is omitted from the fit due to onset of detector saturation. The accidental counts increase with a slope of 2.42, which is consistent with $N_{\mathrm{acc}} \propto (N_{\mathrm{pair,i}} + N_{\mathrm{R,i}} + N_{\mathrm{dark}}/\eta_{\mathrm{i}})(N_{\mathrm{pair,s}} + N_{\mathrm{R,s}} + N_{\mathrm{dark}}/\eta_{\mathrm{s}})$, where N_{dark} is the dark counts, $N_{\mathrm{pair},u}$ is the counts from four-wave mixing, $N_{\mathrm{R},u}$ is the counts from SpRS, and η_u is the detector efficiency in channel u [6]. Since N_{pair} is quadratic in power, N_{R} is linear in power, and N_{dark} is constant, N_{acc} has a fourth-order polynomial dependence on pump power. The fit indicates that we are in the region, where the second-order term is dominant. Notice also that the coincidence counts are 1-3 orders of magnitude larger than the accidental coincidence counts. The free-carrier absorption becomes significant only when the pump power exceeds 50 mW, and we thus neglect its impact in the considered regime [39].

In addition, we define the brightness B of our photon-pair source according to [40]

$$B = \frac{N_{\mathrm{cc}}}{P_{\mathrm{p}}\Delta t \Delta\lambda}, \tag{2}$$

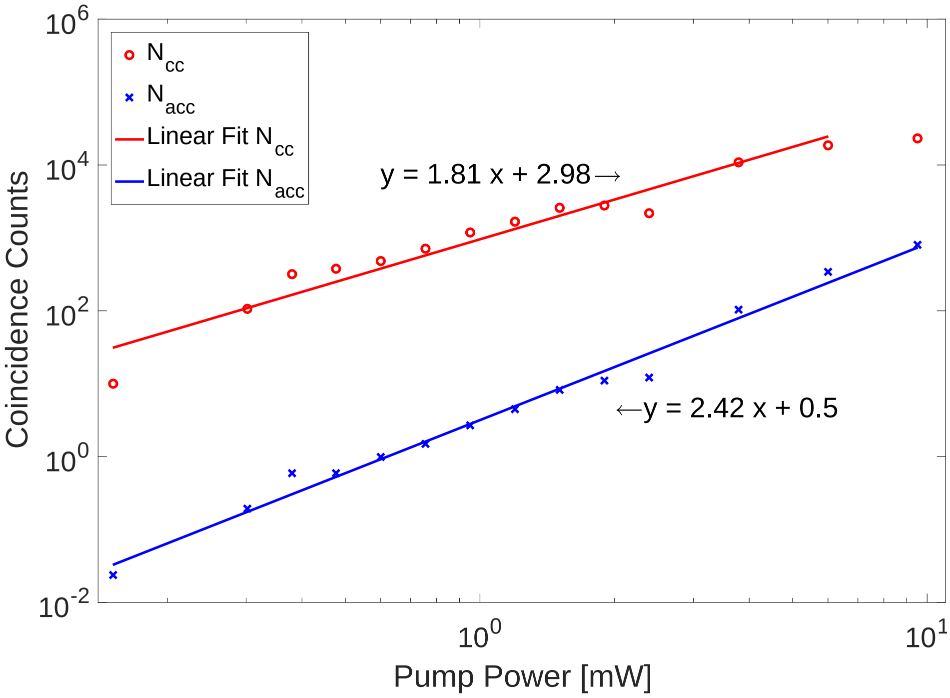

Fig. 3. Coincidence counts and accidental coincidence counts showing approximately quadratic behavior. All points are obtained from 600 s measurements. In the linear fits $y = \log_{10}(N_{cc})$ and $x = \log_{10}(P_p/\text{mW})$.

where $N_{cc}/\Delta t$ is the measured coincidence-count rate in the time window Δt, and $\Delta\lambda$ is the FWHM of the wavelength channels of 0.4 nm. At a pump power of $P_p = 1$ mW, where the obtained CAR is approximately 400, the measured brightness of our source is $B_{det} = 5\ (\text{s mW nm})^{-1}$. By accounting for all losses succeeding the silicon waveguide (output PCGC, AWGs, TBPFs and SPDs), we estimate the internal, i.e. in-waveguide, photon-pair brightness as $B_{est} = B_{det}/(\alpha_s\alpha_i)$, where $\alpha_{s(i)}$ is the combined collection efficiency in the signal (idler) path [40]. With a total estimated loss of 22.7 dB and 23.1 dB in the signal and idler arm, respectively, we find $B_{est} = 1.9 \times 10^5\ (\text{s mW nm})^{-1}$. This internal brightness is comparable to what has previously been demonstrated in silicon strip waveguides [8]. Moreover, our brightness is on the same order of magnitude as sources based on slow-light enhanced waveguides, since these, despite an increased nonlinearity, suffers from higher waveguide losses [37, 15].

To ensure that the source is operating in the single-photon regime, the heralded second-order correlation function $g_H^{(2)}(\tau)$ is measured by adding a 50/50 coupler into the idler arm, see dashed lines in Fig. 1. An extra detector (ID220), with dark count rate of 1 kHz, dead time of 10 μs and a detection efficiency of 20 %, is employed in the extra idler arm. The signal side detector H is used as the heralding reference, while the idler side detectors are called A

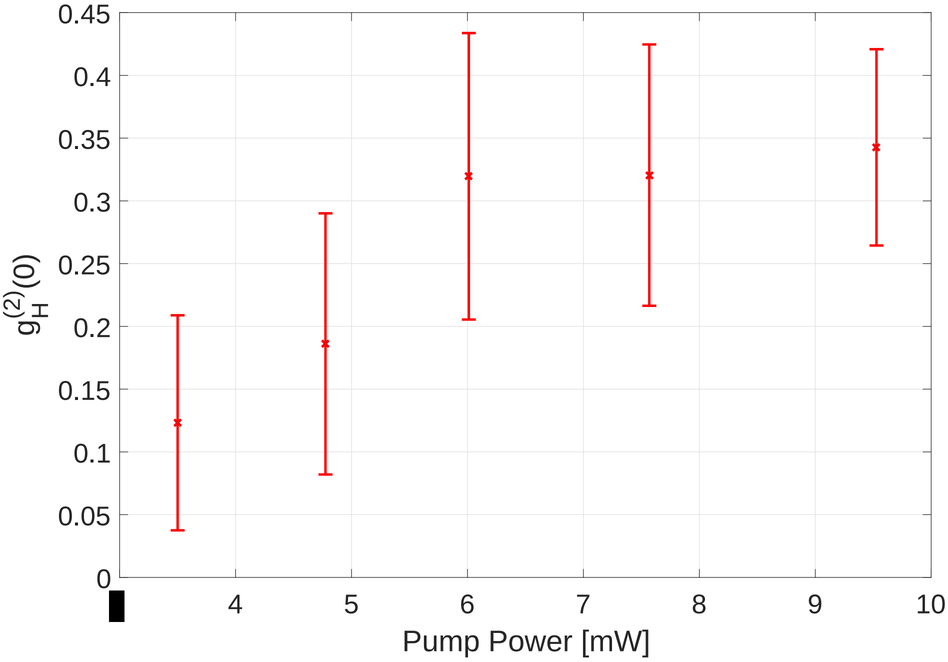

Fig. 4. Heralded second-order correlation as a function of pump power at zero delay, $\tau = 0$. Error bars are given as the standard error calculated using Poissonian statistics.

and B, respectively. The second-order correlation function $g_{\mathrm{H}}^{(2)}(\tau)$ is given as [15]

$$g_{\mathrm{H}}^{(2)}(\tau) = \frac{N_{\mathrm{H}} N_{\mathrm{HAB}}(\tau)}{N_{\mathrm{HA}} N_{\mathrm{HB}}(\tau)}, \tag{3}$$

where τ is the relative time delay between detectors A and B, N_{H} is the signal photon count, N_{HA} is the coincidence counts between detectors H and A, N_{HB} is the coincidence counts between detectors H and B, and N_{HAB} is the triple count events between all three detectors.

The second-order correlation function at zero relative time delay $g_{\mathrm{H}}^{(2)}(0)$ is measured for varying pump power and shown in Fig. 4. At all pump powers $g_{\mathrm{H}}^{(2)}(0)$ is less than 0.5, indicating that the source is operating in the single-photon regime[44]. The value of $g_{\mathrm{H}}^{(2)}(0)$ decreases with pump power with the lowest obtained value $g_{\mathrm{H}}^{(2)}(0) = 0.12$ at 3.5 mW pump power. To ensure that the coincidence window encompasses all three detectors, the coincidence window is 2.5 ns, while the detector timing jitter is 300 ps, and the temporal width of the heralded photon wavepacket is estimated to be around 10 ps. At a nonlinear phase shift of $\Phi_{\mathrm{NL}} = 0.02$ using 10 mW of pump power, noise photons are thought to be the main contribution to the non-zero value of $g_{\mathrm{H}}^{(2)}(0)$. The relatively large coincidence window increases the risk of coincidence events resulting from these noise photons.

To investigate the variation of $g_{\mathrm{H}}^{(2)}(\tau)$ the time delay τ was controlled by increasing or decreasing the fiber length in the coupler arm of detector B. The results of this is seen in

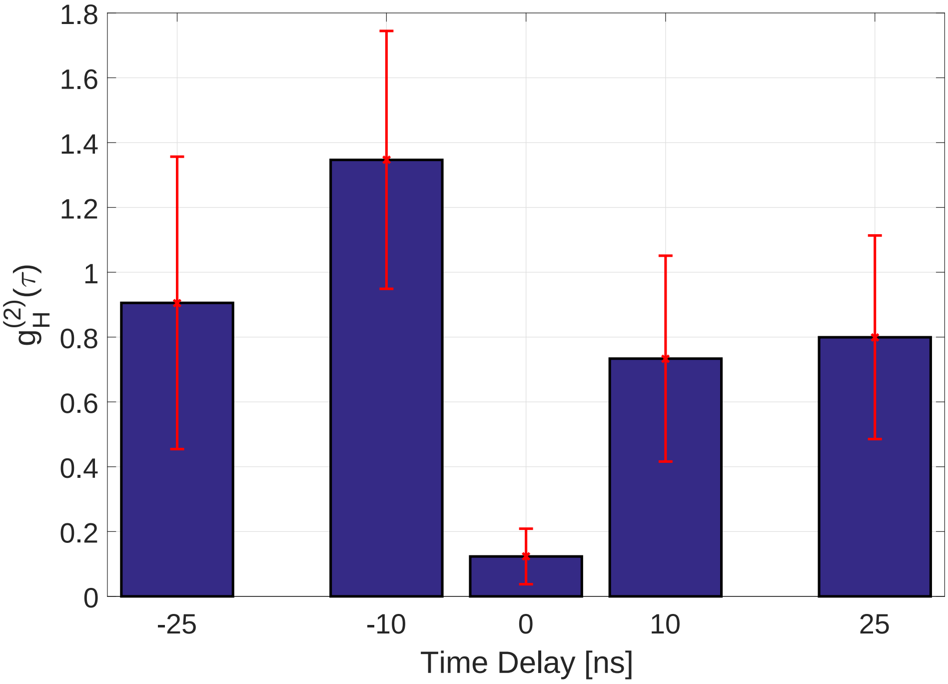

Fig. 5. Second-order correlation function at 3.5 ± 0.5 mW pump power.

Fig. 5. Due to coupling drift during the time-consuming measurements, the pump power was measured to vary between 3 mW and 4 mW. For our measurements performed at non-zero delay, i.e. $\tau = \pm 10$ ns and $\tau = \pm 25$ ns, the value of $g_{\mathrm{H}}^{(2)}(\tau)$ is unity within the error bars, as expected in the asymptotic limit.

Although the experiments in this work demonstrate how thorough suppression of various noise sources enables an ultra-low noise photon-pair source from a silicon straight waveguide, it presently comes at the cost of relatively low coincidence count rates. This issue can, in future work, be mitigated by integrating efficient on-chip filtering [41] and using SPDs exhibiting low dead time and near-unity efficiency [42, 43].

In conclusion, we have demonstrated a CW pumped grating-coupled silicon waveguide as a heralded single-photon source. Single-photon operation was demonstrated by measuring a second-order correlation of $g_{\mathrm{H}}^{(2)}(0) = 0.12$. Due to the large suppression of pump leakage and pump side bands, we obtain a CAR of 673, which, to the best of our knowledge, is the highest reported value for CW-pumped silicon straight waveguides. Photonic crystal based grating couplers were used for on-chip filtering of generated Raman-scattering noise, and in general the low noise contamination in this experiment shows the importance of thorough noise suppression.

Acknowledgments

This work is supported jointly by the China Scholarship Council and the center of excellence: Silicon Photonics for Optical Communications granted by the Danish National Research Foundation (DNRF123).

References

1) L. A. Ngah, O. Alibart, L. Labonté, V. D'Auria, and S. Tanzilli, Laser & Photonics Reviews **9**, L1 (2015).
2) T. Jennewein, M. Barbieri, and A. G. White, Journal of Modern Optics **58**, 276 (2011).
3) F. Kaneda, B. G. Christensen, J. J. Wong, H. S. Park, K. T. McCusker, and P. G. Kwiat, Optica **2**, 1010 (2015).
4) S. Arahira, N. Namekata, T. Kishimoto, H. Yaegashi, and S. Inoue, Optics express **19**, 16032 (2011).
5) J. Fan, A. Migdall, and L. Wang, Optics letters **30**, 3368 (2005).
6) S. D. Dyer, B. Baek, and S. W. Nam, Optics Express **17**, 10290 (2009).
7) J. E. Sharping, K. F. Lee, M. A. Foster, A. C. Turner, B. S. Schmidt, M. Lipson, A. L. Gaeta, and P. Kumar, Optics Express **14**, 12388 (2006).
8) K.-i. Harada, H. Takesue, H. Fukuda, T. Tsuchizawa, T. Watanabe, K. Yamada, Y. Tokura, and S.-i. Itabashi, Optics Express **16**, 20368 (2008).
9) H. Takesue, IEEE Journal of Selected Topics in Quantum Electronics **18**, 1722 (2012).
10) K.-Y. Wang, V. G. Velev, K. F. Lee, A. S. Kowligy, P. Kumar, M. A. Foster, A. C. Foster, and Y.-P. Huang, Optics letters **39**, 914 (2014).
11) J. B. Spring, P. S. Salter, B. J. Metcalf, P. C. Humphreys, M. Moore, N. Thomas-Peter, M. Barbieri, X.-M. Jin, N. K. Langford, W. S. Kolthammer, M. J. Booth, and A. W. Ian, Optics Express **21**, 13522 (2013).
12) C. Xiong, X. Zhang, A. Mahendra, J. He, D.-Y. Choi, C. Chae, D. Marpaung, A. Leinse, R. Heideman, M. Hoekman, C. G. H. Roeloffzen, R. M. Oldenbeuving, P. W. L. van Dijk, C. Taddei, P. H. W. Leong, and B. J. Eggleton, Optica **2**, 724 (2015).
13) C. Xiong, G. D. Marshall, A. Peruzzo, M. Lobino, A. S. Clark, D.-Y. Choi, S. J. Madden1, C. M. Natarajan, M. G. Tanner, R. H. Hadfield, S. N. Dorenbos, T. Zijlstra, V. Zwiller, M. G. Thompson, J. G. Rarity, M. J. Steel, B. Luther-Davies, B. J. Eggleton, and J. L. OBrien, Applied Physics Letters **98**, 051101 (2011).
14) P. Kultavewuti, E. Y. Zhu, L. Qian, V. Pusino, M. Sorel, and J. S. Aitchison, Optics Express **24**, 3365 (2016).
15) A. S. Clark, C. Husko, M. J. Collins, G. Lehoucq, S. Xavier, A. De Rossi, S. Combrié, C. Xiong, and B. J. Eggleton, Optics letters **38**, 649 (2013).
16) R. Soref, IEEE Journal of selected topics in quantum electronics **12**, 1678 (2006).
17) J. Leuthold, C. Koos, and W. Freude, Nature Photonics **4** (2010).

18) T. Liang and H. Tsang, Applied physics letters **85**, 3343 (2004).
19) J. L. Zhang, H. Ishiwata, T. M. Babinec, M. Radulaski, K. Müller, K. G. Lagoudakis, C. Dory, J. Dahl, R. Edgington, V. Soulière, G. Ferro, A. A. Fokin, P. R. Schreiner, Z. X. Shen, N. A. Melosh, and J. Vučković, Nano letters **16**, 212 (2015).
20) X. Ding, Y. He, Z. Duan, N. Gregersen, M. Chen, S. Unsleber, S. Maier, C. Schneider, M. Kamp, S. Höfling, C. Lu, and J. Pan, Physical review letters **116**, 020401 (2016).
21) I. Ali-Khan, C. J. Broadbent, and J. C. Howell, Physical review letters **98**, 060503 (2007).
22) S. Clemmen, K. P. Huy, W. Bogaerts, R. G. Baets, P. Emplit, and S. Massar, Optics Express **17**, 16558 (2009).
23) M. Davanco, J. R. Ong, A. B. Shehata, A. Tosi, I. Agha, S. Assefa, F. Xia, W. M. Green, S. Mookherjea, and K. Srinivasan, Applied Physics Letters **100**, 261104 (2012).
24) I. A. Walmsley and M. G. Raymer, Science **307**, 1733 (2005).
25) K. N. Cassemiro, K. Laiho, and C. Silberhorn, New Journal of Physics **12**, 113052 (2010).
26) W. Tittel, J. Brendel, N. Gisin, and H. Zbinden, Physical Review A **59**, 4150 (1999).
27) Q. Zhang, H. Takesue, S. W. Nam, C. Langrock, X. Xie, B. Baek, M. M. Fejer, and Y. Yamamoto, Optics Express **16**, 5776 (2008).
28) S. Dong, Q. Zhou, W. Zhang, Y. He, W. Zhang, L. You, Y. Huang, and J. Peng, Optics Express **22**, 359 (2014).
29) S. Dong, L. Yu, W. Zhang, J. Wu, W. Zhang, L. You, and Y. Huang, Scientific reports **5** (2015).
30) T. Zhong, H. Zhou, R. D. Horansky, C. Lee, V. B. Verma, A. E. Lita, A. Restelli, J. C. Bienfang, R. P. Mirin, T. Gerrits, S. W. Nam, F. Marsili, M. D. Shaw, Z. Zhang, L. Wang, D. Englund, G. W. Wornell, J. H. Shapiro, and F. N. C. Wong, New Journal of Physics **17**, 022002 (2015).
31) C. Reimer, L. Caspani, M. Clerici, M. Ferrera, M. Kues, M. Peccianti, A. Pasquazi, L. Razzari, B. E. Little, S. T. Chu, D. J. Moss, and R. Morandotti, Optics Express **22**, 6535 (2014).
32) J. M. Arrazola and V. Scarani, Phys. Rev. Lett. **117**, 250503 (2016).
33) C. Jiarui, P. Ziwen, W. Tie-Jun, W. Sihai, and W. Chuan, Int. J. Quantum Inform. **14**, 1650043 (2016).
34) Y. Ding, H. Ou, and C. Peucheret, Optics letters **38**, 2732 (2013).
35) M. Dinu, F. Quochi, and H. Garcia, Applied Physics Letters **82**, 2954 (2003).

36) A. B. Fallahkhair, K. S. Li, and T. E. Murphy, Journal of Lightwave Technology **26**, 1423 (2008).
37) C. Xiong, C. Monat, A. S. Clark, C. Grillet, G. D. Marshall, M. J. Steel, J. Li, L. O'Faolain, T. F. Krauss, J. G. Rarity, and B. J. Eggleton .
38) Q. Lin, F. Yaman, and G. P. Agrawal, Physical Review A **75**, 023803 (2007).
39) D. Dimitropoulos, R. Jhaveri, R. Claps, J. Woo, and B. Jalali, Applied Physics Letters **86**, 071115 (2005).
40) Y. Li, Z.-Y. Zhou, D.-S. Ding, and B.-S. Shi, Optics Express **23**, 28792 (2015).
41) W. Bogaerts, S. K. Selvaraja, P. Dumon, J. Brouckaert, K. De Vos, D. Van Thourhout, and R. Baets, IEEE journal of selected topics in quantum electronics **16**, 33 (2010).
42) B. Korzh, N. Walenta, T. Lunghi, N. Gisin, and H. Zbinden, Applied Physics Letters **104**, 081108 (2014).
43) L. C. Comandar, B. Fröhlich, J. F. Dynes, A. W. Sharpe, M. Lucamarini, Z. Yuan, R. V. Penty, and A. J. Shields, Journal of Applied Physics **117**, 083109 (2015).
44) X.-s. Ma, S. Zotter, J. Kofler, T. Jennewein, and A. Zeilinger, Physical Review A **83**, 043814 (2011).